CHAPTER-1

Background and Introduction

1.1. Navigating Energy and Environmental Concerns on a Global Scale

The increasing energy demand and the worsening of environment are the two most important issues facing the globe today [1]. Fossil fuels now provide the bulk of the world's energy requirements. This dependency instigates extreme emissions of greenhouse gases including N_2O, CH_4, and CO_2. These emissions have a substantial involvement in pollution, global warming, climate change, and several health hazards [2]. Nations and regions all over the world have joined forces to develop and put into action plans targeted at cutting down on and ultimately getting rid of excessive greenhouse gas emissions in order to address these problems. In addressing the challenges of climate change, the Kyoto Protocol and the Paris Climate Agreement serve as shining examples of international collaboration and dedication [3,4]. The Intergovernmental Panel on Climate Change (IPCC) reports that, by 2050, the aggregate global temperatures must not cross the 2 °C increase far pre-industrial levels, as per international agreement [5]. Reducing the use of fossil fuels and the ensuing drop in carbon emissions is essential to achieving this aim. Although nuclear power and renewable energy have advanced significantly, their uptake has not accelerated sufficiently to reduce the need on fossil fuels notably. Reducing the quantity of carbon emitted into the atmosphere still depends on using fewer fossil fuels. While nuclear and non-conventional energy sources have grown gradually, their expansion has not been quick enough to substantially lessen the need on fossil fuels. The U.S. Energy Information Administration (EIA) projects that between 2010 and 2050, the world's energy consumption would rise by around 50 %, as shown in **Figure 1.1 (a)** [6]. Even though the amount of fossil fuels used has significantly decreased, oil still makes up the majority of the world's energy consumption, i.e., 31.2 %, accompanied by coal (27.2 %) and

natural gas (24.7 %). However, as **Figure 1.1 (b)** shows, just 5.7 % of the global energy consumption is supplied by renewable energy sources. Non-renewable sources supplied 80 % of the world's energy in 2018 and are predicted to provide 68 % by the year 2050. Therefore, it is expected that for the foreseeable future, fossil fuels will continue to import a significant proportion of the world's energy demands. Since fossil fuels produce large amounts of particulate matter, SO_x, and CO_2 into the environment, their use must be limited [7]. CO_2 emissions are predicted to rise by around 3 % each year [8]. Because CO_2 consumes the infrared radiation from sunlight, the median temperature of the earth rises as a result. To fulfill present and future energy needs while lowering greenhouse gas emissions, new technology development is crucial. Cleaner and renewable energy alternatives are being investigated and put out as viable options for effective energy supplies in an effort to lessen reliance on fossil fuels.

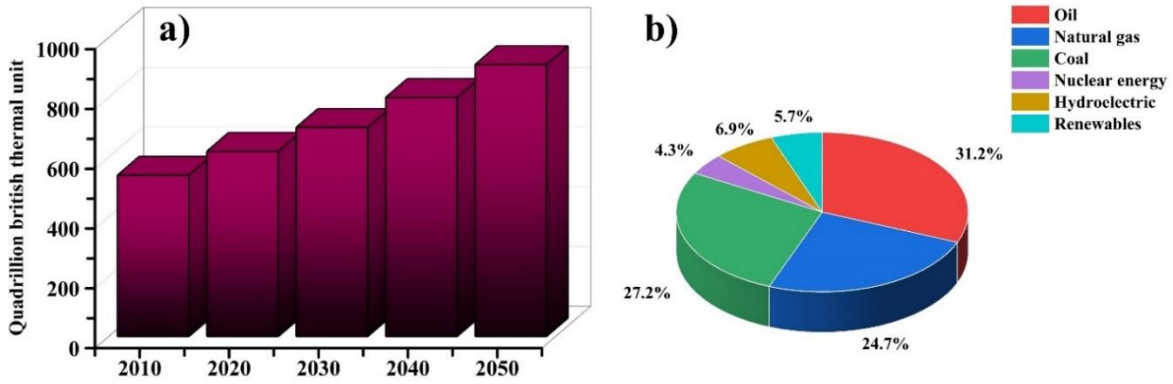

Figure 1.1 (a) Predicted global energy burning projections (Source: U.S. Energy Information Administration, International Energy Outlook 2019). **(b)** gross power usage worldwide by sector in 2023 (Source: Forbes, The BP Statistical assessment regarding Global Energy's highlights 2023).

1.2. Renewable Energy Sources

The report "Future of the Sea: Biological Responses to Ocean Warming" emphasized that the average sea surface temperature is increased by 0.7 °C from the pre-industrial period (1870-1899) to 2005-2014 [9]. As a result of continuous greenhouse gas emissions, it is predicted that this warming trend will continue and that the projected rise in the temperature of the sea surface by 2100 will range from 1.2 to 3.2 °C worldwide [9]. Renewable Energy Sources (RES) such as geothermal, hydroelectric, solar, wind, and hydrogen production via water splitting (H_2 and O_2) offer clean and sustainable alternatives that could significantly lessen our dependency on non-renewable energy sources in light of the rising global energy demands and environmental challenges. RES technologies are being adopted by nations all over the globe in an effort to improve energy independence and tackle the escalating energy dilemma **(Figure 1.2)**. For example, The Indian Prime Minister Narendra Modi and the French President Emmanuel Macron met in Paris on May 4, 2022, to support bilateral collaboration on the development of hydrogen fuels. Wind and solar power are two of the RES that have drawn the most interest from across the world, but owing to their intermittent nature, they need efficient energy management and storage systems, which may be expensive to install. Although it has great potential, geothermal energy is only available in certain areas and may sometimes cause earthquakes. Large amounts of water must be stored for hydroelectric power, which increases the danger of flooding during monsoon seasons.

One especially promising sustainable energy source is hydrogen (H_2). It is produced by the electrochemical process of water splitting, which provides a sustainable and renewable way to produce oxygen and hydrogen. Hydrogen is positioned as a top contender in the switch to

cleaner energy as a result of this technology's growing recognition as a major contributor to the replacement of fossil fuels for energy storage and conversion systems [11].

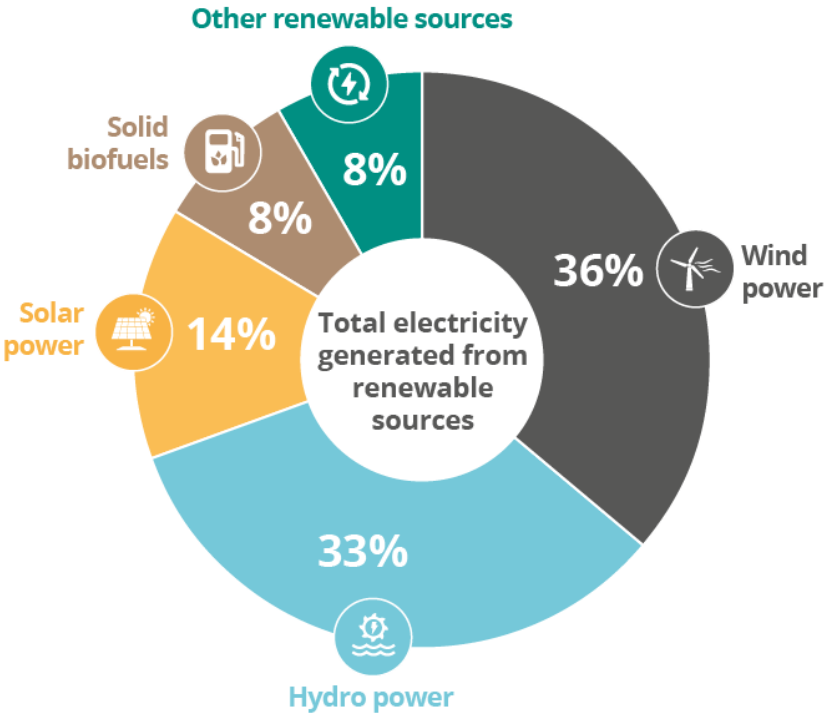

Figure 1.2 Electricity generated from renewable sources [10].

1.3. Electrochemical Water Splitting

Electrocatalysis of water entails the dissociation of water molecules into hydrogen (H_2) and oxygen (O_2) through the application of electricity. Catalysts are employed in an electrochemical cell to reduce the energy needed for this phenomenon, as illustrated schematically in **Figure 1.3**. Water splitting comprises two redox half-cell reactions: the Oxygen Evolution Reaction (OER) at the anode, producing O_2 and the Hydrogen Evolution Reaction (HER) at the cathode, forming H_2. A Proton Exchange Membrane (PEM) serves to

segregate these reactions, facilitating the passage of protons while maintaining the separation of gases in distinct compartments. The electrolysis of water is inherently slow because of the complex multi-electron and proton transfer reactions in the OER and HER. The improvement of potent catalysts is essential for accelerating such reactions and enhancing overall water-splitting efficiency. Noble metals like platinum, ruthenium, and iridium are considered highly effective catalysts for water splitting; however, their scarcity and high-cost limit their widespread use.

The electrolyte employed in water splitting is generally either acidic or alkaline. OER is often conducted in an alkaline environment, while HER is typically conducted in an acidic environment. But in order to accomplish total water splitting, HER and OER need to take place in the same electrolytic environment. While water splitting may be carried out in both alkaline and acidic solutions, alkaline water electrolysis is often used. This preference resulted from the fact that acidic conditions have the potential to destroy the membrane and the electrocatalyst, which might affect the electrolysis system's stability [12]. Because of their ideal operating conditions, alkaline water electrolyzers are already well-established and widely accessible in the commercial market. However, for alkaline electrolysis to be practical, the alkaline HER must proceed efficiently, which is often challenging due to its slow kinetics. Consequently, improving alkaline HER's reaction rate continues to be a key area of attention for developing alkaline water electrolysis technology. The overall reaction intervened in water splitting is represented by **Equation 1.1** as follows:

$$H_2O \longrightarrow H_2 + \frac{1}{2}O_2 \qquad \textbf{(1.1)}$$

Electrochemical water-splitting represents a significant advancement in the production of green hydrogen gas, serving as a clean and high-energy transporter with extensive application possibilities [13]. Nonetheless, the sluggish kinetics and elevated overpotential of the OER considerably diminish the efficacy of water electrolysis. Fuel cells, water-splitting, and metal-air batteries are some of the most direct, effective, and sustainable approaches for energy generation and storage through electrochemical reactions. These systems depend on essential reversible processes, such as the water oxidation reaction (WOR), commonly referred to as OER, along with the oxygen reduction reaction (ORR) and the hydrogen evolution reaction (HER) [14].

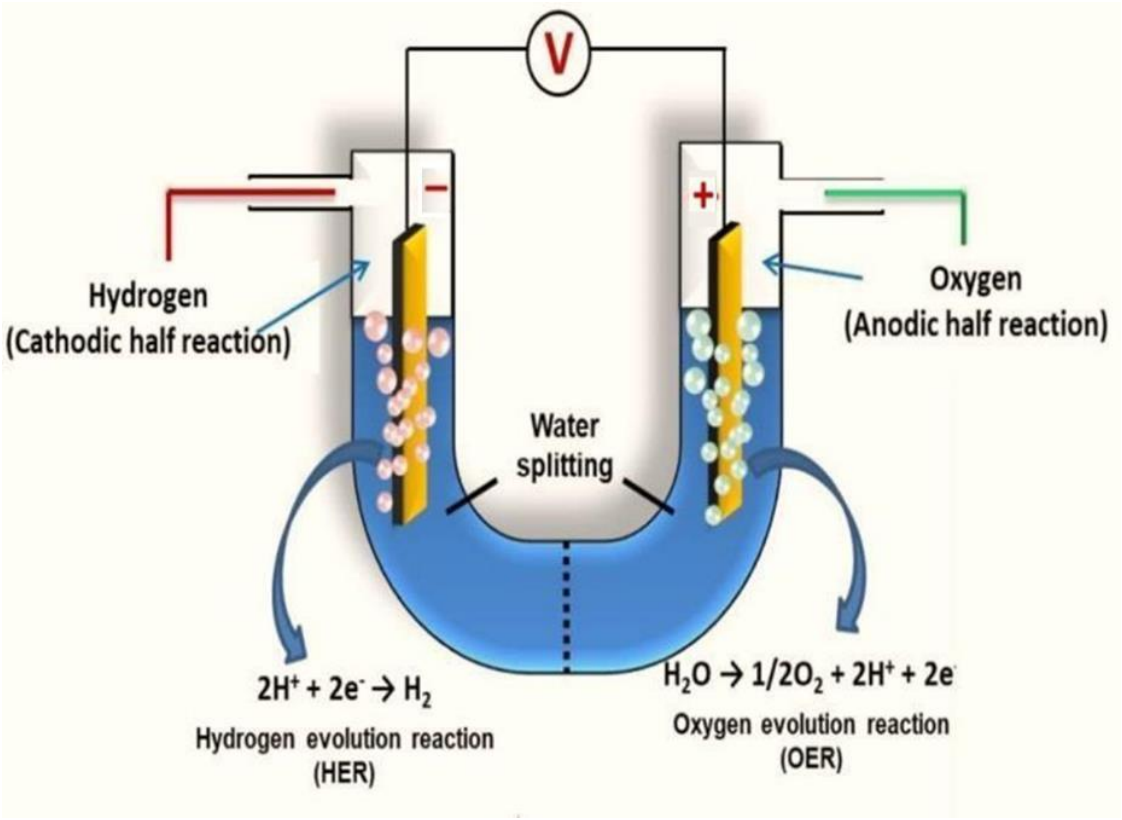

Figure 1.3 Pictorial depiction of electrochemical water splitting.

1.3.1. Water-Splitting Across Different pH Conditions

1.3.1.1. Water-Splitting in neutral medium

Pure water exhibits low electrical conductivity due to its minimal self-ionization, with conductivity approximately one millionth of that of seawater. As a result, pure water electrolysis is a laborious and sluggish process that needs extra energy, provided as overpotential, to get beyond several activation barriers. Without this additional energy, the electrolysis may continue erratically or fail to occur altogether.

The electrolysis of pure water at neutral pH (pH = 7) and at 25 °C is represented by the following reactions (**Equations 1.2, 1.3, and 1.4**):

$2H_2O\ (l) + 2e^- \longrightarrow H_2\ (g) + 2OH^-$ $(E^0 = -0.42\ V)$ (At Cathode) **(1.2)**

$2H_2O\ (l) \longrightarrow O_2\ (g) + 4H^+ + 4e^-$ $(E^0 = +0.82\ V)$ (At Anode) **(1.3)**

Overall Reaction: $2H_2O\ (l) \longrightarrow 2H_2\ (g) + O_2\ (g)$ $(E^0 = -1.24\ V)$ **(1.4)**

The total water electrolysis process is thermodynamically unfavorable due to its negative cell potential. Thus, to start the process, an external voltage of around 2.4 V is needed. Because of the low ion concentration and difficult electron transport at the electrode interfaces, an overpotential of around 0.6 V at each electrode is also required to maintain the reaction. By adding electrocatalysts and using a suitable electrolyte, such as a salt, acid, or base, to increase conductivity and lower energy barriers, the efficiency of electrolysis may be greatly increased.

1.3.1.2. Water-Splitting in acidic medium

The concentration of hydrogen ions (H^+) rises in the presence of acid, and subsequently, these ions undergo the reduction at the cathode, while water oxidation occurs at the anode. The electrolysis of acidic electrolyte (pH < 7) and at 25 °C is represented by the following reactions (**Equations 1.5, 1.6, and 1.7**):

$2H^+ + e^- \longrightarrow H_2\,(g)$ ($E^0 = +0.0$ V) (At Cathode) **(1.5)**

$2H_2O\,(l) \longrightarrow O_2\,(g) + 4H^+ + 4e^-$ ($E^0 = +1.23$ V) (At Anode) **(1.6)**

Overall reaction: $2H_2O\,(l) \longrightarrow 2H_2\,(g) + O_2\,(g)$ ($E^0 = -1.23$ V) **(1.7)**

The whole reaction has a negative standard electrode potential (E^0), making the process thermodynamically unfavorable. In contrast to pure water, the reaction occurs at a markedly reduced potential, hence increasing its viability in acidic environments.

1.3.1.3. Water-splitting in basic medium

Under alkaline environments, the production of excess hydroxide ions (OH^-) enhances the oxidation process at the anode, where these ions discharge electrons and generate O_2. Simultaneously, water molecules at the cathode undergo reduction to generate H_2. The reactions occur as outlined under alkaline conditions (pH > 7) at 25 °C (**Equation 1.8, 1.9 and 1.10**).

$2H_2O\,(l) + 2e^- \longrightarrow H_2\,(g) + 2OH^-$ ($E^0 = -0.83$ V) (At Cathode) **(1.8)**

$4OH^- \longrightarrow O_2\,(g) + 2H_2O + 4e^-$ ($E^0 = +0.4$ V) (At Anode) **(1.9)**

Overall reaction: $2H_2O\,(l) \longrightarrow 2H_2\,(g) + O_2\,(g)$ $(E^0 = -1.23\ V)$ **(1.10)**

1.4. Oxygen Evolution Reaction

The OER, often referred to as the water oxidation reaction, represents a significant challenge in water splitting, as its slow kinetics inherently restrict the efficacy of energy conversion [15]. The process at the anode, known as OER, entails the creation of the O=O (O_2) bond through a series of four proton-coupled electron transfer steps [16–18]. These multiple steps generate various reaction intermediates, which contribute to a high overpotential and sluggish reaction kinetics. The OER exhibits a strong dependence on pH, and its equilibrium half-cell potential (E_a^0) at 1 atm and 298 K (25 °C), referenced against the standard hydrogen electrode (SHE) or normal hydrogen electrode (NHE), can be articulated by following **Equations 1.11, 1.12, and 1.13**:

At pH = 0; $2H_2O\,(l) \longrightarrow O_2\,(g) + 4H^+ + 4e^-$; $E_a^0 = 1.23\ V$ **(1.11)**

At pH = 7; $2H_2O\,(l) \longrightarrow O_2\,(g) + 4H^+ + 4e^-$; $E_a^0 = 0.817\ V$ **(1.12)**

At pH = 14; $4OH^- \longrightarrow O_2\,(g) + 2H_2O + 4e^-$; $E_a^0 = 0.404\ V$ **(1.13)**

1.4.1. Mechanism in OER

The Adsorbate Evolution Mechanism (AEM) and the Lattice Oxygen Mechanism (LOM) are two mechanisms that elucidate the process of the OER on catalyst surfaces. Both methods are essential for understanding the behavior of OER catalysts and enhancing their effectiveness. AEM in acidic circumstances depends on the adsorption of water molecules and the generation of oxygen-containing intermediates directly on the catalyst surface, culminating in the release

of O_2 **(Figure 1.4)**. LOM in acidic circumstances entails the direct involvement of oxygen atoms from the catalyst's crystal lattice in the synthesis of the O-O bond **(Figure 1.4)**. This technique is characteristic of catalysts where lattice oxygen may be readily mobilized and oxidized. AEM in a basic medium entails the adsorption of hydroxide ions (OH^-) on the catalyst surface and the sequential generation of oxygen-containing intermediates that ultimately yield O_2 **(Figure 1.5)**. The active sites of the catalyst promote the adsorption and conversion of these intermediates. In LOM, lattice oxygen atoms from the catalyst's crystalline structure immediately engage in the creation of the O-O bond, resulting in O_2 evolution **(Figure 1.5)**. This method entails the oxidation of lattice oxygen and the creation of oxygen vacancies, distinguishing it from AEM, where all oxygen is derived from water or hydroxide ions.

1.4.1.1. The Conventional Adsorbate Evolution Mechanism (AEM)

According to the established electrochemical mechanism (AEM), the OER contains four main phases, each requiring the conduction of four protons and electrons, in both acidic and alkaline conditions. In an acidic environment, O_2 gas is created by the oxidation of water molecules, simultaneously creating four protons (H^+) and four electrons (e^-). In contrast, in alkaline circumstances, O_2 is generated from the oxidation of hydroxide ions (OH^-) into water (H_2O), followed by the transfer of four electrons.

Water is initially adsorbed onto the active site (M) in the first step, where it then undergoes one electron transfer to create the hydroxyl intermediate species **(Equation 1.14 and 1.15)**.

$$H_2O + M \longrightarrow M\text{-}OH_{ads} + H^+ + e^- \quad \text{(in acid)} \qquad \textbf{(1.14)}$$

$$OH^- + M \longrightarrow M\text{-}OH_{ads} + e^- \quad \text{(in base)} \qquad \textbf{(1.15)}$$

The second step might be undergone with an electrochemical oxide route through another electron conduction **(Equation 1.16 and 1.17)**.

$$M\text{-}OH_{ads} \longrightarrow M\text{-}O_{ads} + H^+ + e^- \text{ (in acid)} \qquad \textbf{(1.16)}$$

$$M\text{-}OH_{ads} + OH^- \longrightarrow M\text{-}O_{ads} + H_2O + e^- \text{ (in base)} \qquad \textbf{(1.17)}$$

The last phase involves the fusion of two intermediary species to produce O_2, which is then released **(Equation 1.18)**.

$$2M\text{-}O_{ads} \longrightarrow 2M + O_2 \qquad \textbf{(1.18)}$$

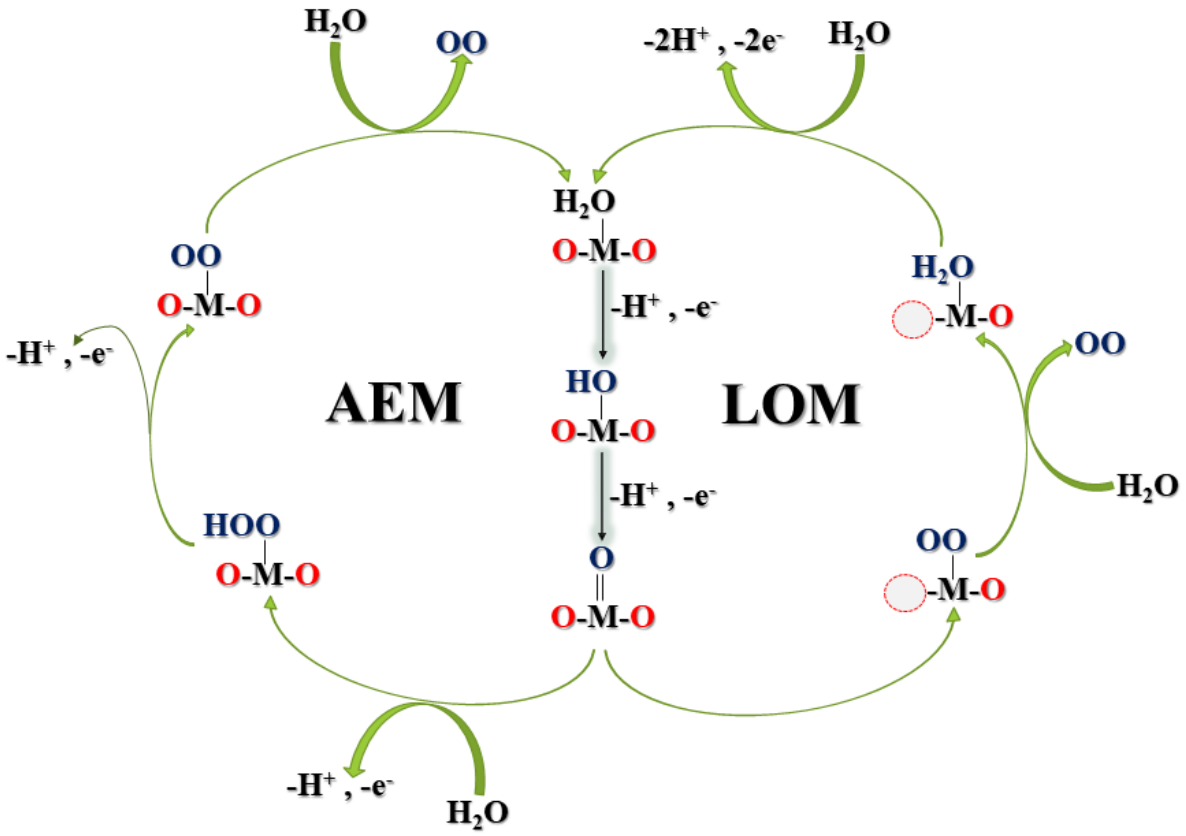

Figure 1.4 Plausible mechanism pathways of OER in acidic medium.

1.4.1.2. The Lattice Oxygen Mechanism (LOM)

1.4.1.2.1. In Base

In contrast to the traditional AEM, the lattice oxygen redox reactions that are a part of LOM's non-concerted proton-electron transfer stages display pH-reliant OER activity, which violates the scaling connection [19–22]. The groundbreaking research by Shao-Horn and colleagues provides explicit experimental confirmation for lattice oxygen oxidation in LOM-OER employing members of the perovskite family as catalysts in an alkaline environment (in situ ^{18}O isotope labeling on-line electrochemical mass spectrometry) [23]. In addition to concerted

and non-concerted proton-electron transfer OER processes, it hypothesized an OER mechanism on surface oxygen sites [23]. These are what Kolpak and his coworkers refer to as O_{ads}-O_{latt} mechanisms (OOM) [20]. The active site, which is a lattice oxygen site for OOM and a transition metal site for LOM, is the main distinction between the two. They also discovered that LOM is better for perovskites than OOM. This is due to the fact that OH* intermediates choose the transition metal site over the oxygen site for OER when choosing an adsorption site. The LOM has five fundamental processes, including one chemical step, four electrochemical steps using coordinated proton-electron transfer, and one electrochemical step. With oxygen desorption, the chemical step transforms into an electron-transfer phase, and the final deprotonation process transforms from a concerted proton-electron transfer to a proton-transfer step.

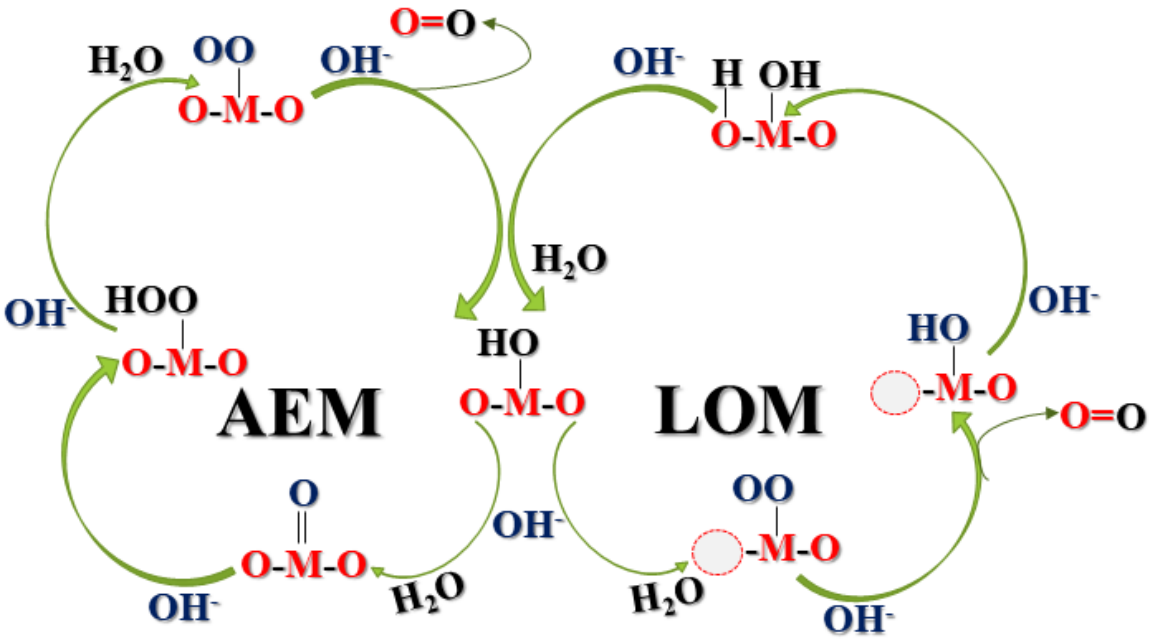

Figure 1.5. Plausible mechanism pathways of OER in basic medium.

1.4.1.2.2. In Acid

By using differential electrochemical mass spectrometry (DEMS), ^{18}O-isotope labeling tests, the LOM is also seen in acid electrolyte [24–26]. Heitbaum and Wohlfahrt-Mehrens, for instance, showed how RuO_2's lattice oxygen contributes to the OER [24]. Comninellis and colleagues found that the uppermost levels of the oxygen lattice at IrO_2 participate in the OER [25]. The OER mechanism, according to Krtil and colleagues, is dependent on the applied voltages. $Ru_{0.9}Ni_{0.1}O_2$ requires potentials greater than 1.12 V vs. SCE (1.42 V vs. RHE) to allow oxygen exchange [26]. In contrast to Heitbaum's or Krtil's groups' findings, Shao-Horn and colleagues discovered that there is no oxygen exchange on the facets of RuO_2 rutile (111), (101), (100), and (110) films [27]. Regardless of such opposing viewpoints, it makes sense to infer LOM routes in acid from what has been discovered in alkaline.

1.4.2. Electrocatalysts for OER in alkaline environment

The OER electrocatalysts speed up the kinetics of the reaction and lower the overpotential [28,29]. RuO_2 and IrO_2, which are based on noble metals, have often been used for OER in acidic environment with high stability and activity [30–33]. Additionally, alloys based on Ru, Ir, and Rh have been investigated to achieve effective OER [34–36]. On the other hand, RuO_2 and IrO_2's OER activity in an alkaline media falls short of realistic standards. Nevertheless, being expensive and availability of rare earth abundance of noble metals limit their widespread practical use [37–39]. Regarding this, transition metal-derived catalysts, such as hydroxides, selenides, sulfides, phosphides, and metal oxides, have been investigated lately with good electrochemical activity and stability for OER reactions [40–49].

1.4.2.1. Oxides

When subjected to an oxidizing potential, metal oxides are more thermodynamically durable than other compounds like sulfides, nitrides, selenides, etc. [50]. These are often split into two major families, namely spinels and perovskites, due to their most prevalent crystalline structure. The oxygen ions adhere to a cubic, closely packed geometry with four octahedral and eight tetrahedral sites per formula unit in spinel-kind materials with the common formula AB_2O_4. Perovskites are uncommon materials having a cubic structure that have the general formula ABO_3. The other most prevalent non-cubic versions of oxides are the tetragonal and orthorhombic phases [51].

1.4.2.1.1. Fe containing spinels

Fe is the most prevalent of the transition metals, making it a very desirable element for use as an inexpensive OER catalyst [52]. Because they are less active toward the OER than Co-based catalysts, Fe and Fe-doped catalysts have a disadvantage [53]. However, it was suggested that structural variations and accessible surface areas may be the primary causes of variances in activity among the various metals, independent of other aspects [53]. This makes it possible to alter the design of Fe-based catalysts by synthesis, that can help to close the performance gap between the transition metal oxides and Fe [54]. For instance, Ni-Fe layered double hydroxide (LDH) hierarchical hollow nanoprisms possess a large specific surface area of 245 $m^2 g^{-1}$ and a significant catalytic performance with η_{10} for the OER of just 280 mV vs. RHE (1 M KOH, 25 °C) [55]. Other useful forms possess consistently developed nanosheets [56] or strongly oriented flake array structures [57], on the substrate's surface. A straightforward Fe_3O_4 catalyst

produced an η_{10} of 438 mV vs. RHE at 25 °C and 1 M KOH [58]. For spinel structures (AB_2O_4), an Fe-based catalyst has shown good performance.

A significant portion of this category includes transition metal ferrites, which have the conventional formula MFe_2O_4 (M = Co, Zn, Cu, Ni etc.) and possess a number of intriguing features, including a low toxicity, high electric conductivity, rich redox chemistry, ease of synthesis, and cheap expense [59]. Spinel is a bimetallic substance, therefore substituting another metal for it may change the conductivity of ferrites. This is due to the fact that the aforementioned electron hopping caused redox shifts between the ions Fe^{2+} and Fe^{3+}, which led to the electrical conductivity of ferrites [60]. There may be an oxygen deficit in the crystal lattice as a result of few lattices oxygen escaping out of the oxide during the sintering process. Fe^{3+} is then reduced to Fe^{2+} in order to compensate for the electrical charge generated in the lattice unit. The generation of extra Fe^{2+} ions in the solution is accelerated by this reduction, increasing the hopping rate of electrons in ferrites [60].

1.4.2.2. Selenides

Transition metal chalcogenides are currently being widely employed for numerous purposes, notably photovoltaics and high-temperature superconductors. Additionally, they were used in heterogeneous catalysis to convert methylenecyclopropanes to cyclobutanones by oxidative ring expansion utilizing H_2O_2 as the oxidant. Currently, selenides have been explored in the field of HER electrocatalysis. Owing to such bifunctional behavior, they constitute a further fascinating set of substances appropriate with respect to the OER. The structural diversity of selenides together with increased electrical characteristics are extremely suitable to continually

adjusting of the electrocatalyst activity. In addition, the intriguing OER electrocatalytic functionalities of Cu, Fe, Mn, Mo, Co, or Ni-based selenides could be enhanced even more [61]. Selenides are considered for having better both the catalytic activity and the OER performance than metal oxides, owing to the lesser electronegativity of Se (2.55) in comparison with elemental O (3.44) [62]. This ends up resulting to the enhancement of catalyst activation, enhanced covalency in the metal–chalcogenide link and the initiation of the OER catalysis by decreasing the redox potential of the catalytic site [63]. The approximate η_{10} for diverse selenides with either Fe, Ni, or Co cation yields an average overpotential of roughly 300 mV [61,64,65]. There was a rise in catalytic efficiency after doping with an extra component. For instance, doping CoSe with P, Ni, Cu, or Fe [65–67] shown to be advantageous. For Co–Fe–Se, its enhanced functionality is attributed to Fe and Co being in octahedral site that displays stronger catalytic functionality than tetrahedral site. Contrarily, Cu has a greater degree of activity in tetrahedral coordination [68].

Selenides, along with phosphides, operate as “pre-catalysts” for the OER in high alkaline medium. Findings reveal that at the catalyst's facade, some of the Ni from NiSe transforms into NiOOH, serving as the OER catalyst in real time [69]. NiSe constitutes the catalyst’s core that increases the electron conduction in between the electrode substrate and the active layer. If the material is doped with Co or Fe, the framework of $Ni_xM_{1-x}OOH$ (where M = Co, Fe, or other metal) develops, boosting the functionality substantially. This is in accordance with the least overpotentials being demonstrated by Ni-Fe-Se nanostructured material [70]. Nanostructured selenides (nanowrinkles, nanowire arrays) have received substantial interest owing to their noteworthy electrocatalytic functionality. The extremely

robust nanostructured catalysts which have been previously described are generated by either hydrothermal/solvothermal or electro-deposition development of nanostructured catalysts on the required support electrodes. The reactivity of such selenides may be considerably boosted by incorporating the dopant using multiple substances.

1.4.2.3. Polymers as a conducting support material

Polymers have become an increasingly important category of materials in catalysis, primarily because of their adaptable nature, which allows for straightforward adjustments to their morphology and physico-chemical characteristics. In the last ten years, there has been a notable increase in the exploration of conductive polymers for various commercial uses, such as sensors [71,72], conducting wires [73], and antistatic coatings [74]. Metals have been effectively integrated into conductive polymer matrices using techniques like electrochemical deposition especially for electrocatalytic applications. However, the role of conductive polymers as supports for metal catalysts in catalytic processes is still not widely investigated, with only a few studies addressing this area.

This growing interest in conductive polymers is largely driven by their ability to provide a tunable platform for catalytic applications. Conductive polymers present numerous benefits compared to conventional support materials, including their intrinsic electrical conductivity, straightforward functionalization, and the possibility of achieving a high surface area. The characteristics of these materials render them especially appealing for improving the efficacy of noble metal catalysts, frequently employed in HER and OER processes. Moreover, the capacity to alter the polymer's structure enhances the management of catalyst dispersion,

stability, and interaction with reactants, which could result in enhanced catalytic efficiency and selectivity.

1.4.2.3.1. Polypyrrole

The conducting polymer polypyrrole (ppy) has garnered interest as a possible material for the OER because of its unique blend of chemical stability, electrical conductivity, and ease of synthesis and modification. To ensure that electrons are transferred efficiently between the electrode and the OER intermediates, ppy offers a conductive conduit for electrons. Ohmic drop during electrochemical processes are minimized with the aid of good electrical conductivity, which is essential for OER. The surface area that is accessible for catalytic reactions may be increased by the formation of a porous structure by polypyrrole. A larger surface area makes more OER active sites possible, increasing the reaction's catalytic effectiveness. Metal catalysts that are known to be active for OER, such as cobalt, nickel, iron, or their oxides or hydroxides, are often supported by ppy. In order to assure a greater number of active sites, the polymer matrix may aid in dispersing metal nanoparticles, increasing their distribution, and minimizing agglomeration.

Polypyrrole (ppy) is a good alternative for electrochemical applications because it has a number of benefits over other conducting polymers for OER. Its intrinsic qualities, which include its high conductivity, chemical stability, simplicity of synthesis, and tunability, are the source of these advantages. When doped properly, ppy has greater electrical conductivity than several other conducting polymers, including polyaniline (PANI) and polythiophene (PT). Because it enables effective electron transmission between the electrode and the OER

intermediates, conductivity is essential for OER. Although many conducting polymers break down in the extreme OER conditions, especially in alkaline or acidic media, polypyrrole is more stable in alkaline environments than polythiophene and poly(3,4-ethylenedioxythiophene) (PEDOT) substitutes. This makes ppy a better fit for OER since the reaction often takes place at high pH levels. High working potentials are necessary for OER, and polypyrrole can tolerate these circumstances longer than certain other conducting polymers because of its relatively stable electrochemical structure. Other conducting polymers may oxidize or break down structurally more rapidly. ppy may be synthesized in a variety of morphologies, unlike certain other polymers that have limited structural design flexibility (e.g., films, fibers, nanotubes). By adjusting the surface area and porosity of these structures, additional active sites for OER may be provided, increasing overall catalytic efficiency.

1.4.3. Key Parameters for Evaluating OER Activity

Any reaction's overall effectiveness and performance are largely determined by the catalyst. However, selecting the right electrolyte and assessing certain kinetic parameters are only two of the many aspects that must be carefully taken into account for achieving the best catalytic reactivity. Further understanding of the reaction processes and the intrinsic activity of the catalyst depends on critical factors such as electrochemically active surface area (ECSA), Tafel slope, and overpotential.

The OER efficiency is directly impacted by overpotential, which is the additional energy required for undergoing the reaction above and beyond the theoretical voltage. A catalyst that is more efficient has a smaller overpotential. On the other hand, the Tafel slope

offers details regarding the kinetics of the reaction, namely the step that determines the rate and how the reaction rate varies with the applied voltage. Faster electron transfer kinetics and more advantageous reaction conditions are indicated by a lower Tafel slope.

Assessing the number of active sites on the catalyst exterior also needs an understanding of the electrochemically active surface area or ECSA. Because a larger ECSA offers more sites for the reaction to occur, it usually corresponds with increased catalytic activity. Taken as a whole, these factors are essential for deciphering how various materials or situations affect the reaction route and for comprehending the behavior of OER catalysts.

Such characteristics will be thoroughly discussed in the next sections, emphasizing their significance in assessing and maximizing catalyst performance for OER.

1.4.3.1. Electrolyte and Electrode

The characteristics of the working electrode and electrolyte possess a considerable significance impact on the efficiency of electrochemical processes, particularly the OER. The electrode substrate's wettability, conductivity, and structural properties all have an impact on the rate of reaction. Electrode supports are commonly split into two sections depending on their surface structure and electrolyte movement: flat surface electrodes and three-dimensional (3D) electrodes. The smooth, planar surface of flat surface electrodes, such glassy carbon (GC), copper/titanium foil (Cu/Ti foil), and fluorine-doped tin oxide (FTO), permits one-sided electrolyte diffusion, which may restrict mass transfer and catalytic activity. Further, 3D electrodes, like nickel foam (NF), carbon cloth (CC), and carbon paper (CP), have a porous

structure that offers several channels for electrolyte access from different directions. Choosing the right electrode support is essential for maximizing reaction efficiency.

The efficiency of electrode materials is significantly affected by electrolytes, as the catalytic activity varies greatly in various electrolyte conditions. Alkaline media are very helpful for the OER, whereas neutral electrolytes provide significant difficulties and acidic environment often lead to subpar catalytic activity. Consequently, the formation of stable electrocatalysts in alkaline environments has elevated to the top of the research priority list. The search for stable electrocatalysts that function well in alkaline conditions is receiving a lot of attention. High stability in alkaline media is shown by a variety of materials, such as carbon-based compounds, hybrid materials, spinels, perovskites, and metal-organic frameworks (MOFs). However, because of their high oxidation potentials, a lot of these materials find it difficult to remain stable in acidic environments.

1.4.3.2. Overpotential (η)

As a crucial measure of an electrocatalyst's effectiveness in promoting electrochemical processes, overpotential is a significant characteristic that describes its catalytic activity [75–80]. To be more precise, overpotential is the extra potential required to support an electrochemical process above and beyond its reversible potential **(Figure 1.6)**. The following **Equation 1.19** can be used to calculate the overpotential for the OER for a given current density.

$$\eta_{OER} = (E_{RHE} - 1.23)\ V \qquad \textbf{(1.19)}$$

For effective catalysis, a more active electrocatalyst is indicated by a lower overpotential. Geometric current density of 10 mA cm^{-2} can be used as a standard reference point for comparing different electrocatalysts' overpotentials and, consequently, catalytic activity. Higher mass loading electrocatalysts might sometimes be tested at current densities of 50 and 100 mA cm^{-2} [81–84].

Since the majority of electrocatalytic functionalities are measured using a three-electrode setup, which may contribute considerable solution resistance (R_s) [75,85], the idea of iR compensation is essential when studying polarization curves. Consequently, by adding the observed solution resistance and accounting for the iR drop, the real overpotential needed for OER is found. The expression for the iR-compensated overpotential is as follows **(Equation 1.20)**:

$$\eta_{OER} = (E_{RHE} - 1.23 - E_{iR})\ V \qquad \textbf{(1.20)}$$

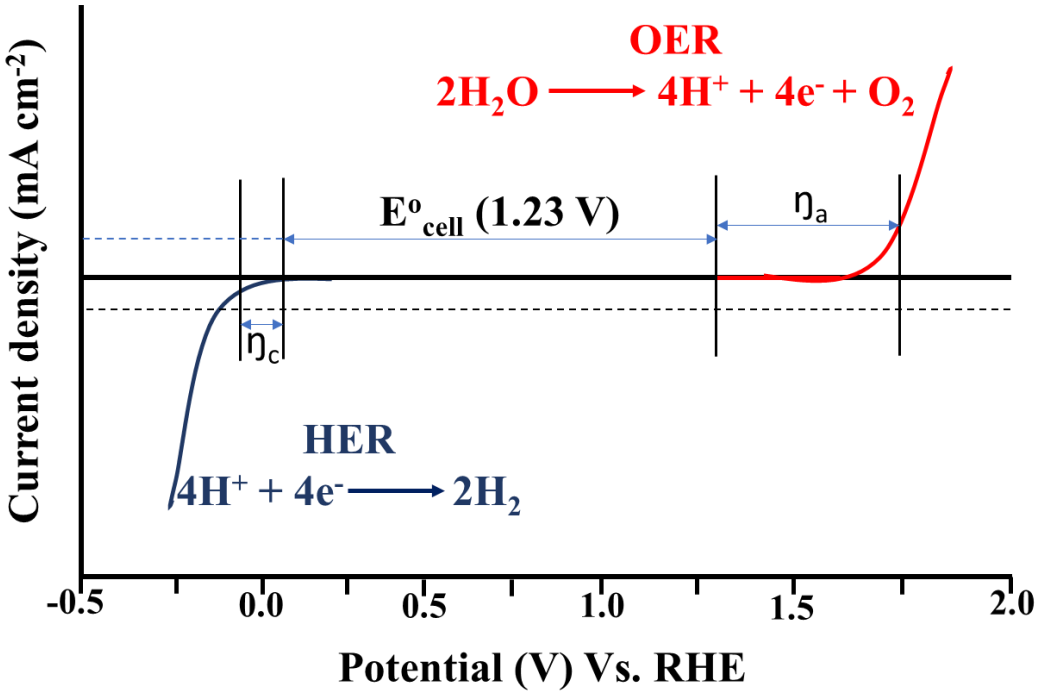

Figure 1.6 i-E curve for HER and OER.

1.4.3.3. Tafel Slope (b)

An essential component of assessing the reaction kinetics related to the OER is the Tafel slope analysis [86,87]. The Tafel equation, which may be written as follows **(Equation 1.21)**, is the source of the Tafel slope:

$$\ln j = \ln j_0 + \left[\frac{\alpha_A nF}{RT}\right]\eta \qquad \textbf{(1.21)}$$

In this equation, j represents the current density, η is the overpotential, F is Faraday's constant, n is the number of electrons transported, α_A is the charge transfer coefficient, T is the absolute temperature, and R is the gas constant. The Tafel slope can be elucidated by plotting log j against η. The slope of the resultant line is provided by $d\log j/d\eta = 2.303RT/\alpha_A nF$. It is

noteworthy that there exists a contrary correlation between the charge transfer coefficient (α_A) and the Tafel slope [75,85]. Improved charge transfer capacities are shown by a smaller Tafel slope, which implies quicker OER kinetics. But it's still difficult to pinpoint the precise mechanism only by looking at the Tafel plots because of the OER's intricate nature, which includes many reaction stages. This emphasizes the need of using complementary analytical methods for completely understanding the kinetics and processes behind the OER.

1.4.3.4. Electrochemically active surface area (ECSA)

Usually, the current density normalized to the electrode's geometric area represents the catalytic performance of a catalyst. As an alternative, it may be adjusted to match the catalyst material's surface area. When measuring the surface area of non-porous materials, atomic force microscopy (AFM) is often used; for high surface area materials, gas adsorption methods, such as nitrogen or hydrogen adsorption, are used. Nevertheless, these techniques are unable to identify areas of the surface that are accessible to the electrolyte or to discriminate between conductive and non-conductive regions [88,89].

In order to solve this, it is thought that a better measure for linking a catalyst's structural characteristics to its electrochemical performance is its electrochemically active surface area (ECSA). Specific capacitance (C_s) and double-layer capacitance (C_{dl}) are used to determine ECSA **(Equation 1.22)**.

$$ECSA = \frac{C_{dl}}{C_s} \times S \qquad \textbf{(1.22)}$$

Where S is geometrical surface area of the working electrode and C_s is specific capacitance and is found to be 40-60 μF cm^{-2} for a smooth surface [90,91].

By choosing a non-faradaic area, doing cyclic voltammetry (CV) at varying scanning, and charting the variation between cathodic and anodic current densities vs. scan rates, one may determine C_{dl}. The C_{dl} value is obtained by dividing the slope of this plot by two **(Equation 1.23)**.

$$C_{dl} = \frac{\Delta j}{2dV_b} \qquad \textbf{(1.23)}$$

This also gives you the value of roughness factor which is also a measure of active sites present and can be calculated using **Equation 1.24**.

$$R_f = \frac{C_{dl}}{C_s} \qquad \textbf{(1.24)}$$

A greater C_{dl} value indicates a larger ECSA. Because various catalysts behave differently electrochemically, comparing catalytic activity across different materials may be difficult. Nevertheless, comparing catalysts that are comparable under the same circumstances yields more accurate findings.

1.4.3.5. Reaction order (p)

In the field of chemical kinetics, the reaction order (p) is determined with the use of a specific partial derivative **(Equation 1.25)**,

$$P = \left(\frac{\partial \log v}{\partial \log Ci}\right) \qquad \textbf{(1.25)}$$

This quantifies how the reaction rate (v) varies with respect to the concentration of a particular species in solution, while maintaining constant conditions for the concentrations of all other reactants, as well as temperature and pressure.

In electrochemistry, the reaction order (p) is defined in a manner comparable to that in traditional chemical kinetics. In addition to maintaining constant temperature and pressure, it is essential to ensure a stable electrode potential throughout the measurement process.

To ascertain the reaction order in electrochemical systems, it is essential to perform a series of current-potential (i-E) measurements at different concentrations of the electroactive species, all while keeping the temperature constant. Using these measurements, we construct plots of log j against log [OH^-] at different fixed potentials across the catalyst/solution interface. The gradients of these linear plots indicate the reaction order concerning the concentration of the species.

Throughout this process, it is crucial to acknowledge that alterations in the double layer structure might take place, particularly at reduced concentrations of the reactant. These alterations can influence the kinetics of the electrode and result in erroneous evaluations of the reaction order. To address this issue, it is essential to ascertain the reaction order under conditions that maintain a consistently high ionic strength in the solution. This approach will help reduce changes in the double layer and ensure accurate kinetic measurements.

1.4.3.6. Standard Electrochemical energy of activation ($\Delta H_{el}^{0\neq}$)

The minimal energy barrier that has to be crossed in order for the reaction to continue on the electrode surface under applied potential is known as the electrochemical energy of activation

for OER. It is a crucial metric that affects the effectiveness of the electrocatalysts used in this process and sheds light on the kinetics of the OER.

When analyzing the temperature dependence of the reaction rate in an electrochemical reaction, the energy of activation is usually found by Arrhenius analysis. A plot showing the log j vs. 1/T at a constant overpotential may be created by carrying out Tafel polarization measurements at various temperatures. Using the Arrhenius equation **(Equation 1.26)**, the activation energy (E_a or $\Delta H_{el}^{0\neq}$) is determined by the slope of this linear plot,

$$k = Ae^{-Ea/RT} \qquad \textbf{(1.26)}$$

Where, k is the rate constant,

A is the pre-exponential factor,

E_a is the activation energy,

R is universal gas constant (8.314×10^{-3} kJ $mol^{-1}K^{-1}$),

T is the absolute temperature.

The inherent kinetic barriers of the OER process are revealed by the electrochemical activation energy, which also indicates how sensitive the reaction rate is to temperature variations. A catalyst that facilitates the OER more efficiently and makes it easier for the reaction to continue at a given applied voltage is indicated by a lower activation energy. A larger activation energy, on the other hand, indicates that the reaction is more kinetically inhibited and needs more energy to proceed at the intended pace.

The creation of effective OER catalysts, especially those based on non-noble metals, depends on comprehending and optimizing the electrochemical energy of activation, since this

directly affects the catalysts' performance in real-world uses such metal-air batteries and water electrolysis. Energy conversion efficiency may be improved by lowering the activation energy, increasing the viability of OER processes for renewable energy systems.

1.4.3.7. Standard Electrochemical enthalpy of activation ($\Delta H^{0\neq}$)

One important measure of the change in enthalpy, or heat content, connected to the production of the activated complex during the OER process at an electrode surface is the electrochemical enthalpy of activation. It sheds light on the energy obstacles that must be removed in order for the reaction to occur when an electric potential is introduced. A popular adaptation of the transition state theory (TST) for electrochemical processes is the enthalpy of activation ($\Delta H^{0\neq}$) **(Equation 1.27)**.

$$\Delta H_{el}^{0\neq} = \Delta H^{0\neq} - \alpha F \eta \qquad \textbf{(1.27)}$$

Where, $\Delta H_{el}^{0\neq}$ is standard electrochemical energy of activation,

$\Delta H^{0\neq}$ is the standard enthalpy of activation,

α is the transfer coefficient,

F is faraday constant (96.5 kJ mol^{-1}),

η is the overpotential (at which activation energy is calculated),

For the calculation of transfer coefficient **(Equation 1.28)**,

$$\alpha = 2.303RT/bF \qquad \textbf{(1.28)}$$

Where, b is the tafel slope,

The value of transfer coefficient is calculated according to the above equation at different temperatures and then the average is taken for further calculation of standard enthalpy of activation ($\Delta H^{0\neq}$).

The energy barrier needed to change from the reactant state to the activated complex when an applied voltage is present is reflected in the enthalpy of activation. Higher reaction rates are often associated with a lower enthalpy of activation, which suggests that the electrocatalyst is more efficient in promoting the reaction and needs less energy to reach the transition state. On the other hand, a greater enthalpy of activation indicates a less effective catalytic process as it requires more energy for the OER to happen.

Due to its direct correlation with the inherent catalytic activity of materials, this characteristic is essential in the design and optimization of catalysts. Researchers may assess the efficiency of various catalysts for the OER by measuring the enthalpy of activation. This is particularly useful for creating less expensive substitutes for conventional noble metal catalysts like IrO_2 and RuO_2. Comprehending $\Delta H^{0\neq}$ aids in locating substances capable of attaining elevated OER activity with reduced energy consumption, thus enhancing the effectiveness of electrochemical devices like metal-air batteries and water electrolyzers used in renewable energy systems.

1.4.3.8. Standard electrochemical entropy of activation ($\Delta S^{0\neq}$)

In particular, when adsorption stages are involved on the catalyst surface, the conventional electrochemical entropy of activation ($\Delta S^{0\neq}$) offers insights into the degree of disorder or

randomness connected with the development of the transition state during the OER process. Understanding the changes in molecular orientation and mobility that occur as reactants travel from their starting state to the activated complex on the electrode surface depends on this crucial characteristic. Typically, the Eyring equation **(Equation 1.29)**, which is derived from transition state theory (TST) and is especially helpful in electrochemical reactions, is used to compute the entropy of activation.

$$\Delta S^{0\neq} = 2.3R\,[\log j + \Delta H_{el}^{0\neq} / 2.3RT - \log (nF\omega C_{OH^-})] \qquad \textbf{(1.29)}$$

Where, $\Delta S^{0\neq}$ is the standard entropy of activation,

j is the current density at overpotential,

n is the no. of electron transfer which is 4 e^- for OER process,

ω is the frequency term (= k_BT/h),

C_{OH^-} is the hydroxide ion concentration,

k_B is the Boltzmann constant,

h is the planck constant.

The adsorption of intermediates such as OH^-, O*, and OOH* onto the catalyst surface plays a crucial role in the mechanism of OER. The reaction between the reactants and the electrode surface determines the entropy shift that occurs throughout this process. A negative entropy might indicate that the intermediates take on a more rigid orientation when adhering

to the electrode, hence decreasing their degrees of freedom. Strong adsorption processes, in which the intermediates form a stable complex with the surface, are illustrated by this. The trend of increasing negative entropy changes ($\Delta S^{0\neq}$) across different catalysts suggests that the catalyst promote more ordered and rigid adsorption of reaction intermediates onto their surfaces. A more negative $\Delta S^{0\neq}$ indicates a greater loss in entropy, which is typically associated with a reduction in the degrees of freedom of the adsorbed species. This can be interpreted as the intermediates adopting a more constrained or well-aligned orientation upon binding to the catalyst surface. Such behavior is indicative of strong adsorption interactions, where intermediates form stable surface complexes, thereby minimizing configurational entropy. A positive entropy might point to a more flexible binding to the catalyst surface where the intermediates maintain some freedom of motion or a more flexible binding to the catalyst surface.

1.4.3.9. Stability

Typically, chronoamperometry (CA) or chronopotentiometry (CP) is adopted for understanding the stability of an electrocatalyst for the OER. In CA, at a constant applied potential, the current density produced by the electrocatalyst is tracked over time [92–96]. Under CA measurements, transition metal-based electrocatalysts often show remarkable stability, sustaining constant current densities for protracted periods of time. Comparatively, CP entails monitoring the potential at a constant current density throughout time [97,98]. Generally, current densities of 10, 20, 50, or 100 mA cm^{-2} are used in order to assess the electrocatalyst's long-term stability under operating settings. An electrocatalyst's stability is

further investigated using cyclic voltammetry. The optimal catalyst exhibits great cyclic durability over many cycles without experiencing a discernible drop in overpotential or current density. This thorough stability assessment guarantees the catalyst's dependability over extended electrochemical reactions.

1.5. Objectives and scope of the thesis

It is now essential to switch to renewable energy sources in the quest for a future devoid of fossil fuels. The ability to harvest and store renewable energy as well as transform it into different forms that may be used requires crucial parts including fuel cells, rechargeable metal-air batteries, and water splitting. The OER is a key component of these technologies since it makes it easier to produce pure oxygen. However, a major obstacle to the widespread use of these energy devices is the innately sluggish kinetics of OER.

OER is a far more complicated process than the HER, needing a much larger overpotential in order to obtain the same current density. This creates a significant energetic barrier to effective OER operation. Even though noble metal oxides like IrO_2 and RuO_2 are regarded as benchmark OER catalysts, there is still a critical need to find more affordable substitutes. Even though a variety of materials have been investigated for OER catalysis, there is still a lot of unexplored ground to cover.

Because of their potential as OER catalysts, spinel oxides especially bimetallic and trimetallic compounds and mixed metal chalcogenides have attracted a lot of attention lately. These materials have benefits including ease of synthesis, which creates new opportunities for the development of effective and inexpensive electrocatalysts. Further, when these materials

are incorporated in the conducting polymer matrix, they can show synergistic advancement in their catalytic activity. Moreover, the main objective of the thesis, is to investigate the polypyrrole composites for the catalysts of OER and the study of fundamental kinetic and thermodynamic parameters, which are important to examine the catalytic activity. In light of OER's significance for renewable energy systems and the field's recent developments, the following goals are the focus of this thesis:

1. Using egg white as a precursor during the thermal decomposition process, the goal of this research is to synthesize zinc ferrite ($Zn_xFe_{3-x}O_4$) nanoparticles with varying stoichiometric compositions (x = 0.25, 0.5, 0.75, and 1) and to systematically assess their electrocatalytic performance for the OER. The objective is to examine the effects of varying zinc-to-iron ratios on the catalytic activity and efficiency of the produced nanoparticles, with a focus on determining the ideal composition for best results. Through the analysis of important performance measures, such as the current density at a given overpotential and the Tafel slope, which sheds light on the reaction kinetics, the research seeks to identify the composition that produces the best electrocatalytic efficiency. Furthermore, *operando* spectro-electrochemical methods will be used in the investigation to get real-time absorption spectra while the OER is in progress. This will make it possible to look more closely at the active species and reaction intermediates involved, which will improve our comprehension of the underlying processes controlling the electrocatalytic activity of the produced zinc ferrite catalysts. By using this strategy, the study hopes to aid in the creation of high-performing, reasonably priced catalysts for OER in applications related to renewable energy sources.

2. Since oxides have been extensively explored, we've attempted to synthesize the other metal chalcogenides and their polypyrrole composites. This work aims to synthesize, analyze, and assess the performance of a manganese selenide (α-MnSe) and polypyrrole (ppy) heterostructure as an electrocatalyst for OER. In order to reach a current density of 10 mA cm^{-2}, an exceptionally low overpotential of 168 mV (vs. RHE) is needed. In order to provide mechanistic insights into the catalytic process, the research also uses *operando* UV-Vis spectro-electrochemical methods to investigate the generation of intermediate species during OER. The research aims to show the potential of this non-noble metal-based electrocatalyst as a highly efficient substitute for OER applications, advancing affordable and sustainable energy technologies by contrasting the performance of this composite with benchmark catalysts composed of manganese and rare earth metals.
3. The objective of this research is to investigate the effects of molybdenum (Mo) doping on the electrocatalytic performance of manganese selenide. The doped material is synthesized using a hydrothermal process, followed by the fabrication of a polypyrrole composite through a solid-state method. This study aims to evaluate the impact of Mo doping on enhancing the catalytic properties, with a particular focus on achieving lower overpotentials. The composite material outperforms its individual counterparts, with preliminary results showing an overpotential of 205 mV (vs. RHE) at a current density of 10 mA cm^{-2}. Additionally, *operando* spectro-electrochemical studies are also conducted to monitor the real-time formation of active intermediates during the OER, providing deeper insights into the mechanistic role of Mo doping in improving catalytic efficiency. This

research seeks to advance the development of highly efficient, non-noble metal-based OER catalysts through strategic metal doping.

4. The objective of this research is to explore the impact of copper (Cu) doping on the electrocatalytic performance of manganese selenide and to compare its catalytic activity with that of molybdenum (Mo) doping. The Cu-doped catalyst is synthesized using a hydrothermal process, followed by composite preparation with polypyrrole through a solid-state method. This study aims to assess how Cu doping influences the OER performance and its catalytic efficiency relative to the Mo-doped and undoped materials. Preliminary results demonstrate that while the Cu-doped manganese selenide catalyst outperforms its individual counterparts, that exhibits a higher overpotential of 299 mV (vs. RHE) to achieve a current density of 10 mA cm^{-2}, indicating that it does not surpass the performance of the Mo-doped variant. Additionally, *operando* spectro-electrochemical studies are conducted to investigate the active intermediates formed during the OER process, offering insights into the mechanistic differences caused by Cu doping. This research aims to deepen the understanding of metal doping strategies for optimizing non-noble metal electrocatalysts for OER applications.

1.6. References

[1] M.A.M. Hasan, Y. Wang, C.R. Bowen, Y. Yang, 2D Nanomaterials for Effective Energy Scavenging, Nano-Micro Lett. 13 (2021). https://doi.org/10.1007/s40820-021-00603-9.

[2] E. Von Schneidemesser, P.S. Monks, Air quality and climate-synergies and trade-offs, Environ. Sci. Process. Impacts. 15 (2013) 1315–1325. https://doi.org/10.1039/c3em00178d.

[3] J. Wentz, UNITED NATIONS FRAMEWORK CONVENTION ON CLIMATE CHANGE, in: Environ. Heal. 21st Century from Air Pollut. to Zoonotic Dis. Vol. 1-2, 2018: bll 604–606. https://scholar.google.com/scholar?hl=en&as_sdt=0%2C5&q=3.%09United+Nations+Framework+Convention+on+Climate+Change%2C+Adoption+of+the+Paris+Agreement%2C+21st+Conference+of+the+Parties%2C+Paris%2C+2015.&btnG= (toegang verkry 14 Augustus 2024).

[4] M. Paterson, Framework Convention on Climate Change, in: Int. Encycl. Environ. Polit., 2014: bll 206–207. https://doi.org/10.4135/9781412963893.n262.

[5] EEA, European Environment Agency – waste prevention – home page, Eur. Environ. Agency. (2015). https://www.eea.europa.eu/en (toegang verkry 14 Augustus 2024).

[6] EIA, International Energy Outlook 2023 - U.S. Energy Information Administration (EIA), EIA. (2023). https://www.eia.gov/outlooks/ieo/ (toegang verkry 26 September 2024).

[7] R.J. Detz, J.N.H. Reek, B.C.C. Van Der Zwaan, The future of solar fuels: When could they become competitive?, Energy Environ. Sci. 11 (2018) 1653–1669. https://doi.org/10.1039/c8ee00111a.

[8] J. Hansen, M. Sato, P. Kharecha, G. Russell, D.W. Lea, M. Siddall, Climate change and trace gases, Philos. Trans. R. Soc. A Math. Phys. Eng. Sci. 365 (2007) 1925–1954. https://doi.org/10.1098/rsta.2007.2052.

[9] M.J. Genner, J.J. Freer, L.A. Rutterford, Future of the Sea: Biological Responses to Ocean Warming Foresight-Future of the Sea Evidence Review Foresight, Government Office for Science Biological Responses to Ocean Warming, in: Futur. Sea Biol. Responses to Ocean Warm., 2017: bll 6–8.

[10] European Environment Agency, A future based on renewable energy — European Environment Agency, (2022). https://www.eea.europa.eu/signals-archived/signals-2022/articles/a-future-based-on-renewable-energy (toegang verkry 28 September 2024).

[11] S. Shiva Kumar, V. Himabindu, Hydrogen production by PEM water electrolysis – A

review, Mater. Sci. Energy Technol. 2 (2019) 442–454. https://doi.org/10.1016/j.mset.2019.03.002.

[12] M. Schalenbach, G. Tjarks, M. Carmo, W. Lueke, M. Mueller, D. Stolten, Acidic or Alkaline? Towards a New Perspective on the Efficiency of Water Electrolysis, J. Electrochem. Soc. 163 (2016) F3197–F3208. https://doi.org/10.1149/2.0271611jes.

[13] S. Anantharaj, S.R. Ede, K. Karthick, S. Sam Sankar, K. Sangeetha, P.E. Karthik, S. Kundu, Precision and correctness in the evaluation of electrocatalytic water splitting: Revisiting activity parameters with a critical assessment, Energy Environ. Sci. 11 (2018) 744–771. https://doi.org/10.1039/c7ee03457a.

[14] M. Tahir, L. Pan, F. Idrees, X. Zhang, L. Wang, J.Z.-N. Energy, undefined 2017, Electrocatalytic oxygen evolution reaction for energy conversion and storage: A comprehensive review, ElsevierM Tahir, L Pan, F Idrees, X Zhang, L Wang, JJ Zou, ZL WangNano Energy, 2017•Elsevier. (n.d.). https://www.sciencedirect.com/science/article/pii/S221128551730294X (toegang verkry 27 September 2024).

[15] M. Rana, S. Mondal, L. Sahoo, K. Chatterjee, P.E. Karthik, U.K. Gautam, Emerging Materials in Heterogeneous Electrocatalysis Involving Oxygen for Energy Harvesting, ACS Appl. Mater. Interfaces. 10 (2018) 33737–33767. https://doi.org/10.1021/acsami.8b09024.

[16] Q. Liang, G. Brocks, A. Bieberle-Hütter, Oxygen evolution reaction (OER) mechanism under alkaline and acidic conditions, JPhys Energy. 3 (2021) 26001. https://doi.org/10.1088/2515-7655/abdc85.

[17] N. Snir, N. Yatom, M. Caspary Toroker, Progress in understanding hematite electrochemistry through computational modeling, Comput. Mater. Sci. 160 (2019) 411–419. https://doi.org/10.1016/j.commatsci.2019.01.001.

[18] J. Rossmeisl, Z.W. Qu, H. Zhu, G.J. Kroes, J.K. Nørskov, Electrolysis of water on oxide surfaces, J. Electroanal. Chem. 607 (2007) 83–89. https://doi.org/10.1016/j.jelechem.2006.11.008.

[19] X. Rong, J. Parolin, A.M. Kolpak, A Fundamental Relationship between Reaction Mechanism and Stability in Metal Oxide Catalysts for Oxygen Evolution, ACS Catal. 6 (2016) 1153–1158. https://doi.org/10.1021/acscatal.5b02432.

[20] J.S. Yoo, X. Rong, Y. Liu, A.M. Kolpak, Role of Lattice Oxygen Participation in Understanding Trends in the Oxygen Evolution Reaction on Perovskites, ACS Catal. 8 (2018) 4628–4636. https://doi.org/10.1021/acscatal.8b00612.

[21] Z.F. Huang, J. Song, Y. Du, S. Xi, S. Dou, J.M.V. Nsanzimana, C. Wang, Z.J. Xu, X. Wang, Chemical and structural origin of lattice oxygen oxidation in Co–Zn oxyhydroxide oxygen evolution electrocatalysts, Nat. Energy. 4 (2019) 329–338.

https://doi.org/10.1038/s41560-019-0355-9.

[22] X. Li, H. Wang, Z. Cui, Y. Li, S. Xin, J. Zhou, Y. Long, C. Jin, J.B. Goodenough, Exceptional oxygen evolution reactivities on CaCoO3 and SrCoO3, Sci. Adv. 5 (2019). https://doi.org/10.1126/sciadv.aav6262.

[23] A. Grimaud, O. Diaz-Morales, B. Han, W.T. Hong, Y.L. Lee, L. Giordano, K.A. Stoerzinger, M.T.M. Koper, Y. Shao-Horn, Activating lattice oxygen redox reactions in metal oxides to catalyse oxygen evolution, Nat. Chem. 9 (2017) 457–465. https://doi.org/10.1038/nchem.2695.

[24] M. Wohlfahrt-Mehrens, J. Heitbaum, Oxygen evolution on Ru and RuO2 electrodes studied using isotope labelling and on-line mass spectrometry, J. Electroanal. Chem. 237 (1987) 251–260. https://doi.org/10.1016/0022-0728(87)85237-3.

[25] S. Fierro, T. Nagel, H. Baltruschat, C. Comninellis, Investigation of the oxygen evolution reaction on Ti/IrO2 electrodes using isotope labelling and on-line mass spectrometry, Electrochem. commun. 9 (2007) 1969–1974. https://doi.org/10.1016/j.elecom.2007.05.008.

[26] K. Macounova, M. Makarova, P. Krtil, Oxygen evolution on nanocrystalline RuO2 and Ru0.9Ni0.1O2-δ electrodes - DEMS approach to reaction mechanism determination, Electrochem. commun. 11 (2009) 1865–1868. https://doi.org/10.1016/j.elecom.2009.08.004.

[27] K.A. Stoerzinger, O. Diaz-Morales, M. Kolb, R.R. Rao, R. Frydendal, L. Qiao, X.R. Wang, N.B. Halck, J. Rossmeisl, H.A. Hansen, T. Vegge, I.E.L. Stephens, M.T.M. Koper, Y. Shao-Horn, Orientation-Dependent Oxygen Evolution on RuO2 without Lattice Exchange, ACS Energy Lett. 2 (2017) 876–881. https://doi.org/10.1021/acsenergylett.7b00135.

[28] X. Li, X. Hao, A. Abudula, G. Guan, Nanostructured catalysts for electrochemical water splitting: Current state and prospects, J. Mater. Chem. A. 4 (2016) 11973–12000. https://doi.org/10.1039/c6ta02334g.

[29] C. Li, J.B. Baek, Recent Advances in Noble Metal (Pt, Ru, and Ir)-Based Electrocatalysts for Efficient Hydrogen Evolution Reaction, ACS Omega. 5 (2020) 31–40. https://doi.org/10.1021/acsomega.9b03550.

[30] C.J. Chang, Y.C. Chu, H.Y. Yan, Y.F. Liao, H.M. Chen, Revealing the structural transformation of rutile RuO2 via in situ X-ray absorption spectroscopy during the oxygen evolution reaction, Dalt. Trans. 48 (2019) 7122–7129. https://doi.org/10.1039/c9dt00138g.

[31] T. Audichon, T.W. Napporn, C. Canaff, C. Morais, C. Comminges, K.B. Kokoh, IrO2 Coated on RuO2 as Efficient and Stable Electroactive Nanocatalysts for Electrochemical Water Splitting, J. Phys. Chem. C. 120 (2016) 2562–2573. https://doi.org/10.1021/acs.jpcc.5b11868.

[32] Y. Lattach, J.F. Rivera, T. Bamine, A. Deronzier, J.C. Moutet, Iridium oxide-polymer nanocomposite electrode materials for water oxidation, ACS Appl. Mater. Interfaces. 6 (2014) 12852–12859. https://doi.org/10.1021/am5027852.

[33] O. Diaz-Morales, S. Raaijman, R. Kortlever, P.J. Kooyman, T. Wezendonk, J. Gascon, W.T. Fu, M.T.M. Koper, Iridium-based double perovskites for efficient water oxidation in acid media, Nat. Commun. 7 (2016). https://doi.org/10.1038/ncomms12363.

[34] T. Reier, M. Oezaslan, P. Strasser, Electrocatalytic oxygen evolution reaction (OER) on Ru, Ir, and pt catalysts: A comparative study of nanoparticles and bulk materials, ACS Catal. 2 (2012) 1765–1772. https://doi.org/10.1021/cs3003098.

[35] T. Zhang, S.A. Liao, L.X. Dai, J.W. Yu, W. Zhu, Y.W. Zhang, Ir-Pd nanoalloys with enhanced surface-microstructure-sensitive catalytic activity for oxygen evolution reaction in acidic and alkaline media, Sci. China Mater. 61 (2018) 926–938. https://doi.org/10.1007/s40843-017-9187-1.

[36] Z. Pu, T. Liu, G. Zhang, H. Ranganathan, Z. Chen, S. Sun, Electrocatalytic Oxygen Evolution Reaction in Acidic Conditions: Recent Progress and Perspectives, ChemSusChem. 14 (2021) 4636–4657. https://doi.org/10.1002/cssc.202101461.

[37] A.K. Singh, S. Ji, B. Singh, C. Das, H. Choi, P.W. Menezes, A. Indra, Alkaline oxygen evolution: exploring synergy between fcc and hcp cobalt nanoparticles entrapped in N-doped graphene, Mater. Today Chem. 23 (2022). https://doi.org/10.1016/j.mtchem.2021.100668.

[38] B. Chakraborty, A. Indra, P. V. Menezes, M. Driess, P.W. Menezes, Improved chemical water oxidation with Zn in the tetrahedral site of spinel-type ZnCo2O4 nanostructure, Mater. Today Chem. 15 (2020). https://doi.org/10.1016/j.mtchem.2019.100226.

[39] D. González-Flores, I. Sánchez, I. Zaharieva, K. Klingan, J. Heidkamp, P. Chernev, P.W. Menezes, M. Driess, H. Dau, M.L. Montero, Heterogeneous water oxidation: Surface activity versus amorphization activation in cobalt phosphate catalysts, Angew. Chemie - Int. Ed. 54 (2015) 2472–2476. https://doi.org/10.1002/anie.201409333.

[40] J. Song, C. Zhu, B.Z. Xu, S. Fu, M.H. Engelhard, R. Ye, D. Du, S.P. Beckman, Y. Lin, Bimetallic Cobalt-Based Phosphide Zeolitic Imidazolate Framework: CoPx Phase-Dependent Electrical Conductivity and Hydrogen Atom Adsorption Energy for Efficient Overall Water Splitting, Adv. Energy Mater. 7 (2017) 6423–6436. https://doi.org/10.1002/aenm.201601555.

[41] J. Yu, T.A. Le, N.Q. Tran, H. Lee, Earth-Abundant Transition-Metal-Based Bifunctional Electrocatalysts for Overall Water Splitting in Alkaline Media, Chem. - A Eur. J. 26 (2020) 6423–6436. https://doi.org/10.1002/chem.202000209.

[42] S. Sanati, A. Morsali, H. García, First-row transition metal-based materials derived

from bimetallic metal-organic frameworks as highly efficient electrocatalysts for electrochemical water splitting, Energy Environ. Sci. 15 (2022) 3119–3151. https://doi.org/10.1039/d1ee03614a.

[43] M.Q. Yang, J. Wang, H. Wu, G.W. Ho, Noble Metal-Free Nanocatalysts with Vacancies for Electrochemical Water Splitting, Small. 14 (2018). https://doi.org/10.1002/smll.201703323.

[44] M.Q. Yang, J. Wang, H. Wu, G.W. Ho, Noble Metal-Free Nanocatalysts with Vacancies for Electrochemical Water Splitting, Small. 14 (2018). https://doi.org/10.1002/smll.201703323.

[45] J. Wang, X. Yue, Y. Yang, S. Sirisomboonchai, P. Wang, X. Ma, A. Abudula, G. Guan, Earth-abundant transition-metal-based bifunctional catalysts for overall electrochemical water splitting: A review, J. Alloys Compd. 819 (2020). https://doi.org/10.1016/j.jallcom.2019.153346.

[46] P.W. Menezes, A. Indra, P. Littlewood, M. Schwarze, C. Göbel, R. Schomäcker, M. Driess, Nanostructured manganese oxides as highly active water oxidation catalysts: A boost from manganese precursor chemistry, ChemSusChem. 7 (2014) 2202–2211. https://doi.org/10.1002/cssc.201402169.

[47] Y. Zhou, S. Sun, C. Wei, Y. Sun, P. Xi, Z. Feng, Z.J. Xu, Significance of Engineering the Octahedral Units to Promote the Oxygen Evolution Reaction of Spinel Oxides, Adv. Mater. 31 (2019). https://doi.org/10.1002/adma.201902509.

[48] R.D.L. Smith, C. Pasquini, S. Loos, P. Chernev, K. Klingan, P. Kubella, M.R. Mohammadi, D. Gonzalez-Flores, H. Dau, Spectroscopic identification of active sites for the oxygen evolution reaction on iron-cobalt oxides, Nat. Commun. 8 (2017). https://doi.org/10.1038/s41467-017-01949-8.

[49] X. Long, Z. Wang, S. Xiao, Y. An, S. Yang, Transition metal based layered double hydroxides tailored for energy conversion and storage, Mater. Today. 19 (2016) 213–226. https://doi.org/10.1016/j.mattod.2015.10.006.

[50] S. Jin, Are Metal Chalcogenides, Nitrides, and Phosphides Oxygen Evolution Catalysts or Bifunctional Catalysts?, ACS Energy Lett. 2 (2017) 1937–1938. https://doi.org/10.1021/acsenergylett.7b00679.

[51] U. Muller, J. Wiley, Inorganic Structural Chemistry., Zeitschrift fur Krist. - New Cryst. Struct. 209 (1994) 564. https://doi.org/10.1524/zkri.1994.209.6.564.

[52] Y. Yan, B.Y. Xia, B. Zhao, X. Wang, A review on noble-metal-free bifunctional heterogeneous catalysts for overall electrochemical water splitting, J. Mater. Chem. A. 4 (2016) 17587–17603. https://doi.org/10.1039/C6TA08075H.

[53] X. Liu, X. Wang, X. Yuan, W. Dong, F. Huang, Rational composition and structural design of in situ grown nickel-based electrocatalysts for efficient water electrolysis, J.

Mater. Chem. A. 4 (2015) 167–172. https://doi.org/10.1039/c5ta07047c.

[54] H. Osgood, S. V. Devaguptapu, H. Xu, J. Cho, G. Wu, Transition metal (Fe, Co, Ni, and Mn) oxides for oxygen reduction and evolution bifunctional catalysts in alkaline media, Nano Today. 11 (2016) 601–625. https://doi.org/10.1016/j.nantod.2016.09.001.

[55] A.M. Atta, A.O. Ezzat, A.M. El-Saeed, M.H. Wahby, M.M.S. Abdallah, Superhydrophobic organic and inorganic clay nanocomposites for epoxy steel coatings, Prog. Org. Coatings. 140 (2020) 105502. https://doi.org/10.1016/j.porgcoat.2019.105502.

[56] P. can Wang, L. Wan, Y. qun Lin, B. guo Wang, NiFe Hydroxide Supported on Hierarchically Porous Nickel Mesh as a High-Performance Bifunctional Electrocatalyst for Water Splitting at Large Current Density, ChemSusChem. 12 (2019) 4038–4045. https://doi.org/10.1002/cssc.201901439.

[57] X. Liu, X. Wang, X. Yuan, W. Dong, F. Huang, Rational composition and structural design of in situ grown nickel-based electrocatalysts for efficient water electrolysis, J. Mater. Chem. A. 4 (2015) 167–172. https://doi.org/10.1039/c5ta07047c.

[58] M. Li, Y. Xiong, X. Liu, X. Bo, Y. Zhang, C. Han, L. Guo, Facile synthesis of electrospun MFe2O4 (M = Co, Ni, Cu, Mn) spinel nanofibers with excellent electrocatalytic properties for oxygen evolution and hydrogen peroxide reduction, Nanoscale. 7 (2015) 8920–8930. https://doi.org/10.1039/c4nr07243j.

[59] S. Diodati, L. Pandolfo, A. Caneschi, S. Gialanella, S. Gross, Green and low temperature synthesis of nanocrystalline transition metal ferrites by simple wet chemistry routes, Nano Res. 7 (2014) 1027–1042. https://doi.org/10.1007/s12274-014-0466-3.

[60] T. Pandiarajan, S. Ravichandran, L.J. Berchmans, Enhancing the electro catalytic activity of manganese ferrite through cerium substitution for oxygen evolution in KOH solutions, RSC Adv. 4 (2014) 64364–64370. https://doi.org/10.1039/c4ra09806d.

[61] A.T. Swesi, J. Masud, M. Nath, Nickel selenide as a high-efficiency catalyst for oxygen evolution reaction, Energy Environ. Sci. 9 (2016) 1771–1782. https://doi.org/10.1039/c5ee02463c.

[62] K. Xu, H. Ding, H. Lv, S. Tao, P. Chen, X. Wu, W. Chu, C. Wu, Y. Xie, Understanding Structure-Dependent Catalytic Performance of Nickel Selenides for Electrochemical Water Oxidation, ACS Catal. 7 (2017) 310–315. https://doi.org/10.1021/acscatal.6b02884.

[63] M. Serhan, M. Sprowls, D. Jackemeyer, M. Long, I.D. Perez, W. Maret, N. Tao, E. Forzani, Total iron measurement in human serum with a smartphone, in: AIChE Annu. Meet. Conf. Proc., 2019: bll 1–3. https://doi.org/10.1039/x0xx00000x.

[64] X. Cao, J.E. Medvedeva, M. Nath, Copper Cobalt Selenide as a High-Efficiency Bifunctional Electrocatalyst for Overall Water Splitting: Combined Experimental and Theoretical Study, ACS Appl. Energy Mater. 3 (2020) 3092–3103. https://doi.org/10.1021/acsaem.0c00262.

[65] J. Masud, W.P.R. Liyanage, X. Cao, A. Saxena, M. Nath, Copper Selenides as High-Efficiency Electrocatalysts for Oxygen Evolution Reaction, ACS Appl. Energy Mater. 1 (2018) 4075–4083. https://doi.org/10.1021/acsaem.8b00746.

[66] J. Zhang, Y. Wang, C. Zhang, H. Gao, L. Lv, L. Han, Z. Zhang, Self-Supported Porous NiSe2 Nanowrinkles as Efficient Bifunctional Electrocatalysts for Overall Water Splitting, ACS Sustain. Chem. Eng. 6 (2018) 2231–2239. https://doi.org/10.1021/acssuschemeng.7b03657.

[67] H. Kang, H. Li, X. Zhao, L. Yang, S. Xu, Anion doped bimetallic selenide as efficient electrocatalysts for oxygen evolution reaction, Ceram. Int. 46 (2020) 2792–2797. https://doi.org/10.1016/j.ceramint.2019.09.270.

[68] X. Cao, E. Johnson, M. Nath, Expanding Multinary Selenide Based High-Efficiency Oxygen Evolution Electrocatalysts through Combinatorial Electrodeposition: Case Study with Fe-Cu-Co Selenides, ACS Sustain. Chem. Eng. 7 (2019) 9588–9600. https://doi.org/10.1021/acssuschemeng.9b01095.

[69] I.H. Kwak, H.S. Im, D.M. Jang, Y.W. Kim, K. Park, Y.R. Lim, E.H. Cha, J. Park, CoSe2 and NiSe2 Nanocrystals as Superior Bifunctional Catalysts for Electrochemical and Photoelectrochemical Water Splitting, ACS Appl. Mater. Interfaces. 8 (2016) 5327–5334. https://doi.org/10.1021/acsami.5b12093.

[70] S. Anantharaj, S. Noda, Nickel selenides as pre-catalysts for electrochemical oxygen evolution reaction: A review, Int. J. Hydrogen Energy. 45 (2020) 15763–15784. https://doi.org/10.1016/j.ijhydene.2020.04.073.

[71] D. Kincal, A. Kumar, A.D. Child, J.R. Reynolds, Conductivity switching in polypyrrole-coated textile fabrics as gas sensors, Synth. Met. 92 (1998) 53–56. https://doi.org/10.1016/s0379-6779(98)80022-2.

[72] J.C. Vidal, E. García, J.R. Castillo, In situ preparation of a cholesterol biosensor: entrapment of cholesterol oxidase in an overoxidized polypyrrole film electrodeposited in a flow system. Determination of total cholesterol in serum, in: Anal. Chim. Acta, 1999: bll 213–222. https://doi.org/10.1016/S0003-2670(98)00838-1.

[73] L.X. Wang, X.G. Li, Y.L. Yang, Preparation, properties and applications of polypyrroles, React. Funct. Polym. 47 (2001) 125–139. https://doi.org/10.1016/S1381-5148(00)00079-1.

[74] C. Jérôme, D. Labaye, I. Bodart, R. Jérôme, Electrosynthesis of polyacrylic/polypyrrole composites: formation of polypyrrole wires, Synth. Met. 101

(1999) 3–4. https://doi.org/10.1016/S0379-6779(98)00524-4.

[75] S. Anantharaj, S.R. Ede, K. Karthick, S. Sam Sankar, K. Sangeetha, P.E. Karthik, S. Kundu, Precision and correctness in the evaluation of electrocatalytic water splitting: Revisiting activity parameters with a critical assessment, Energy Environ. Sci. 11 (2018) 744–771. https://doi.org/10.1039/c7ee03457a.

[76] H.B. Tao, Y. Xu, X. Huang, J. Chen, L. Pei, J. Zhang, J.G. Chen, B. Liu, A General Method to Probe Oxygen Evolution Intermediates at Operating Conditions, Joule. 3 (2019) 1498–1509. https://doi.org/10.1016/j.joule.2019.03.012.

[77] S. Zhao, Y. Wang, J. Dong, C.T. He, H. Yin, P. An, K. Zhao, X. Zhang, C. Gao, L. Zhang, J. Lv, J. Wang, J. Zhang, A.M. Khattak, N.A. Khan, Z. Wei, J. Zhang, S. Liu, H. Zhao, Z. Tang, Ultrathin metal-organic framework nanosheets for electrocatalytic oxygen evolution, Nat. Energy. 1 (2016). https://doi.org/10.1038/nenergy.2016.184.

[78] P.M. Bodhankar, P.B. Sarawade, G. Singh, A. Vinu, D.S. Dhawale, Recent advances in highly active nanostructured NiFe LDH catalyst for electrochemical water splitting, J. Mater. Chem. A. 9 (2021) 3180–3208. https://doi.org/10.1039/d0ta10712c.

[79] S. Anantharaj, S. Kundu, Do the Evaluation Parameters Reflect Intrinsic Activity of Electrocatalysts in Electrochemical Water Splitting?, ACS Energy Lett. 4 (2019) 1260–1264. https://doi.org/10.1021/acsenergylett.9b00686.

[80] M.J. Craig, G. Coulter, E. Dolan, J. Soriano-López, E. Mates-Torres, W. Schmitt, M. García-Melchor, Universal scaling relations for the rational design of molecular water oxidation catalysts with near-zero overpotential, Nat. Commun. 10 (2019). https://doi.org/10.1038/s41467-019-12994-w.

[81] Z. Xue, K. Liu, Q. Liu, Y. Li, M. Li, C.Y. Su, N. Ogiwara, H. Kobayashi, H. Kitagawa, M. Liu, G. Li, Missing-linker metal-organic frameworks for oxygen evolution reaction, Nat. Commun. 10 (2019). https://doi.org/10.1038/s41467-019-13051-2.

[82] C. Cao, D.D. Ma, Q. Xu, X.T. Wu, Q.L. Zhu, Semisacrificial Template Growth of Self-Supporting MOF Nanocomposite Electrode for Efficient Electrocatalytic Water Oxidation, Adv. Funct. Mater. 29 (2019). https://doi.org/10.1002/adfm.201807418.

[83] M. Ding, J. Chen, M. Jiang, X. Zhang, G. Wang, Ultrathin trimetallic metal-organic framework nanosheets for highly efficient oxygen evolution reaction, J. Mater. Chem. A. 7 (2019) 14163–14168. https://doi.org/10.1039/c9ta00708c.

[84] L. Han, J. Xu, X. Zhu, F. Yang, X. Jia, High-performance Ni-V-Fe metal-organic framework electrocatalyst composed of integrated nanowires and nanosheets for oxygen evolution reaction, Mater. Today Energy. 16 (2020). https://doi.org/10.1016/j.mtener.2020.100419.

[85] S. Anantharaj, S. Kundu, Do the Evaluation Parameters Reflect Intrinsic Activity of

Electrocatalysts in Electrochemical Water Splitting?, ACS Energy Lett. 4 (2019) 1260–1264. https://doi.org/10.1021/acsenergylett.9b00686.

[86] S. Anantharaj, S. Noda, M. Driess, P.W. Menezes, The Pitfalls of Using Potentiodynamic Polarization Curves for Tafel Analysis in Electrocatalytic Water Splitting, ACS Energy Lett. 6 (2021) 1607–1611. https://doi.org/10.1021/acsenergylett.1c00608.

[87] T. Shinagawa, A.T. Garcia-Esparza, K. Takanabe, Insight on Tafel slopes from a microkinetic analysis of aqueous electrocatalysis for energy conversion, Sci. Rep. 5 (2015) 23955–6900. https://doi.org/10.1038/srep13801.

[88] C. Wei, S. Sun, D. Mandler, X. Wang, S.Z. Qiao, Z.J. Xu, Approaches for measuring the surface areas of metal oxide electrocatalysts for determining their intrinsic electrocatalytic activity, Chem. Soc. Rev. 48 (2019) 2518–2534. https://doi.org/10.1039/c8cs00848e.

[89] S. Trasatti, O.A. Petrii, Real surface area measurements in electrochemistry, J. Electroanal. Chem. 327 (1992) 353–376. https://doi.org/10.1016/0022-0728(92)80162-W.

[90] A.S. Chaddha, N.K. Singh, M. Malviya, A. Sharma, Birnessite-clay mineral couple in the rock varnish: a nature's electrocatalyst, Sustain. Energy Fuels. 6 (2022) 2553–2569. https://doi.org/10.1039/d2se00185c.

[91] D. Voiry, M. Chhowalla, Y. Gogotsi, N.A. Kotov, Y. Li, R.M. Penner, R.E. Schaak, P.S. Weiss, Best Practices for Reporting Electrocatalytic Performance of Nanomaterials, ACS Nano. 12 (2018) 9635–9638. https://doi.org/10.1021/acsnano.8b07700.

[92] A. Indra, P.W. Menezes, N.R. Sahraie, A. Bergmann, C. Das, M. Tallarida, D. Schmeißer, P. Strasser, M. Driess, Unification of catalytic water oxidation and oxygen reduction reactions: Amorphous beat crystalline cobalt iron oxides, J. Am. Chem. Soc. 136 (2014) 17530–17536. https://doi.org/10.1021/ja509348t.

[93] L. Ding, K. Li, Z. Xie, G. Yang, S. Yu, W. Wang, H. Yu, J. Baxter, H.M. Meyer, D.A. Cullen, F.Y. Zhang, Constructing Ultrathin W-Doped NiFe Nanosheets via Facile Electrosynthesis as Bifunctional Electrocatalysts for Efficient Water Splitting, ACS Appl. Mater. Interfaces. 13 (2021) 20070–20080. https://doi.org/10.1021/acsami.1c01815.

[94] B. Mohanty, P. Bhanja, B.K. Jena, An overview on advances in design and development of materials for electrochemical generation of hydrogen and oxygen, Mater. Today Energy. 23 (2022). https://doi.org/10.1016/j.mtener.2021.100902.

[95] J. Mohammed-ibrahim, H. Moussab, Tuning the electronic structure of the earth-abundant electrocatalysts for oxygen evolution reaction (OER) to achieve efficient alkaline water splitting – A review, J. Energy Chem. 56 (2021) 299–342.

https://doi.org/10.1016/j.jechem.2020.08.001.

[96] Z. Li, Z. Jiang, W. Zhu, C. He, P. Wang, X. Wang, T. Li, L. Tian, Facile preparation of CoSe2 nano-vesicle derived from ZIF-67 and their application for efficient water oxidation, Appl. Surf. Sci. 504 (2020). https://doi.org/10.1016/j.apsusc.2019.144368.

[97] H. Liu, D. Guo, W. Zhang, R. Cao, Co(OH)2 hollow nanoflowers as highly efficient electrocatalysts for oxygen evolution reaction, J. Mater. Res. 33 (2018) 568–580. https://doi.org/10.1557/jmr.2017.390.

[98] J. Cheng, H. Zhang, G. Chen, Y. Zhang, Study of IrxRu1-xO2 oxides as anodic electrocatalysts for solid polymer electrolyte water electrolysis, Electrochim. Acta. 54 (2009) 6250–6256. https://doi.org/10.1016/j.electacta.2009.05.090.